IEEE Access
Multidisciplinary | Rapid Review | Open Access Journal

Received December 12, 2021, accepted December 31, 2021, date of publication January 5, 2022, date of current version February 7, 2022.

Digital Object Identifier 10.1109/ACCESS.2022.3140429

Basis Pursuit With Sparsity Averaging for Compressive Sampling of Iris Images

TARIQ RAHIM[1], (Member, IEEE), RITA MAGDALENA[2], I PUTU AGUS EKA PRATAMA[3], LEDYA NOVAMIZANTI[2,4], (Graduate Student Member, IEEE), I NYOMAN APRAZ RAMATRYANA[1], (Graduate Student Member, IEEE), SOO YOUNG SHIN[1], (Senior Member, IEEE), AND DONG SEONG KIM[1], (Senior Member, IEEE)

[1]Department of IT Convergence Engineering, Kumoh National Institute of Technology, Gumi 39177, Republic of Korea
[2]School of Electrical Engineering, Telkom University, Bandung 40257, Indonesia
[3]Department of Information Technology, Faculty of Engineering, Udayana University, Bali 80361, Indonesia
[4]Human Centric Engineering Research Center, Telkom University, Bandung 40257, Indonesia

Corresponding author: Dong Seong Kim (dskim@kumoh.ac.kr)

This work was supported in part by the Ministry of Science, ICT (MSIT), South Korea, through the Information Technology Research Center Support Program supervised by the Institute for Information Communications Technology Planning and Evaluation (IITP), under Grant IITP-2021-2020-0-01612; and in part by the Priority Research Centers Program through the National Research Foundation of Korea (NRF) through the Ministry of Education, Science and Technology under Grant 2018R1A6A1A03024003.

ABSTRACT This paper proposes novel compressive sampling (CS) of colored iris images using three RGB iterations of basis pursuit (BP) with sparsity averaging (SA), called RGB-BPSA. In RGB-BPSA, a sparsity basis is performed using an average of multiple coherent dictionaries to improve the performance of BP reconstruction. In the experiment, first, the level of wavelet decomposition is studied to analyze the best reconstruction result. Second, the effect of compression rate (CR) is considered. Third, the effect of resolution is investigated. Last, the sparse basis of SA is compared to the existing basis, i.e., curvelet, Daubechies-1 or haar, and Daubechies-8. The superior RGB-BPSA over existing CS is shown by better visual quality with a higher signal-to-noise ratio (SNR) and structural similarity (SSIM) index in the same CR. In addition, reconstruction time also investigated where RGB-BPSA outperforms the curvelet.

INDEX TERMS Compressed sampling, basis pursuit (BP), sparsity averaging, iris images.

I. INTRODUCTION

Medical Imaging (MI) is the science of interpreting or investigating medical obstacles based on several MI processes and digital image processing methods [1]. With the advancement of medical diagnostic equipment, such as magnetic resonance imaging (MRI), ultrasound imaging (UI), computed tomography (CT), iris eye imaging, wireless capsule endoscopy (WCE), and other characteristic medical images are produced in the field of biomedical [2]. Employing those methods, one can generate images of the individual body or each part of its organ for medical science objectives such as diagnosis, treatment, or operation. A lot of research work has been attempted and ongoing for the development of algorithms and systems that can support medical specialists assisting them to enhance the quality of human health. Formulating well-suited and stable algorithms for the investigation of images is the significant challenge that coerces the medical image interpretation fraternity to strive with large efforts [3].

Although medical technologies have led to generating medical data for different parts i.e., both outside and inside of the human body, yet there are issues that need to be addressed. These issues include storage, transmission, and representation in a smaller size with a high level of perceived quality. Taking CT and UI as a case where the number of images produced in one process comprised of more than 55,000 images and quite a large size, respectively make it extremely hard to handle [4]. Similarly, medical data like the iris medical data which is quite sensitive and needs to be of good quality to perform MI analysis. It is vital to adhere to a certain level of quality for these medical data in order to avoid jeopardizing the clinical evaluation. Compression techniques for medical data can help with storage, transmission, and perceived quality issues [5], [6].

The associate editor coordinating the review of this manuscript and approving it for publication was Liangxiu Han.

Compressive sensing or compressive sampling or compressed sensing (CS) was proposed to restore an image or signal when it has been sampled remarkably under the Nyquist rate [7]–[9]. The U.S. Food and Drug Administration approve CS as an approach that break the classic Nyquist rate and reduce the medical investigation time [10]. Recently, CS has opted for the reconstruction of the medical data in detail yet there is a research gap of the iris data analysis where both perceived quality and data representation is of a crucial task. The CS method can assemble data at a below sampling rate, and acquisition of the data along with the compression can be performed in the corresponding process [7].

A. RELATED WORKS

Lately, CS method has been researched briefly for the reconstruction of the signals/images and has achieved satisfactory results considering both theoretical perspectives and engineering applications. These applications span from data like natural to medical to even hyperspectral images [5]. A nonuniform sampling from a sensors has been employed in the CS framework by exploiting the lessened sets of measurements [11]. Nowadays, the data transmitted over wireless networks face two issues i.e., humongous data generation, storage, and transmission. The CS approach has been recently adopted for the reconstruction of the large non-uniformed data generated by sensors using the Fourier transform domain [11]–[13]. CS has also been investigated for the reconstruction of hyperspectral images (HSI), which is based on a multi-type mixing representation conducted at the spectral sampling staging using the CS technique. This technique alleviated the concerns that come with a linear mixed model (LMM), such as the environment, device setups, and tangible nonlinear mixing consequences [14], [15]. Furthermore, a reconstruction of HSI with CS was proposed using the spectral mixing properties where the HSIs are parted into an abundance matrix and endmember matrix using the features of LMM [16]. The conventional CS for HSIs faces issues such as separation and vectorization of the hyperspectral cubes into spectral and special vectors that lead to storage and computational burden in the restoration process. For addressing the above concerns, a CS approach for HSIs is presented via sparse tensor and nonlinear sparse tensor coding [17].

The CS has been lately researched well for MI analysis and has proven to be adequate for the reconstruction. A detailed CS approach based on multiple basis reweighted analysis was proposed for medical data [5]. A CS based on total variation (TV) minimization was presented for the ultrasound CT imaging resulting in lessening the time for acquisition [18]. An active pseudo-polar Fourier-based Radon transform where parallel beaming-based CS approach is adopted for CT images reducing the computational restrains [19]. Moreover, the CS method has drawn attention for CT image restoration dependent on sparseness and sampling tactics [20]–[23]. Similarly, for MRI data, the CS method is researched in detail and demonstrated encouraging outcomes for MRI acquisition speedup [24]–[27]. Deep learning-based CS approaches using vanilla convolutional neural networks [28], ADMM-NET [29], and Generative adversarial networks [30], [31] recently opt for MRI data showing better performance for the reconstruction.

For the WCE and colonoscopy data, CS approach based on TV and average sparsity modelling using basis pursuit denoising is implemented [4]. A 3D discrete cosine transform based image compression approach is implemented addressing the issue of three channels of WCE frame [32]. Some efforts are reported via compression method such as JPEG and MPEG for capsule endoscopic data, yet not favorable due to extreme power dissipation and computational complexities [33]–[36]. Based on our comprehensive research analysis, a specific analysis of spread spectrum (SS) acquisition and BPDN based reconstruction for iris data is not found in the current literature. Consequently, for filling this research gap iris data is employed to investigate as (SS) analysis. The detail behind the motivations and contributions of the particular research work are discussed in subsection II(B).

B. MOTIVATIONS AND CONTRIBUTIONS

The earlier CS methods were based on a sparsity basis using wavelet transform and curvelet [7], [37]. In [38], sparsity analysis prior was proposed using multiple frames with average sparsity prior in radio astronomy images. In [39], sparsity averaging with reweighted analysis (SARA) was proposed for natural images with excessive coherent dictionaries in compressed imaging. Furthermore, multi-basis reweighted analysis was proposed to enhance SARA by using a group of SARA basis for 4 different medical images, i.e., MRI, CT, WCE images, and colonoscopy images [5], [40]. In [5], compressed medical imaging (CMI) was introduced to investigate the performance of the CS method in medical image compression for efficient sampling method. Moreover, a TV-based SARA was proposed for CT images to reduce the reconstruction time of basis pursuit (BP) in SARA [4]. The earlier CMIs are focused on one-layer images and RGB-based CMI is not investigated yet.

Motivated by these, an RGB-based CMI using spread spectrum (SS) and BP with sparsity averaging (RGB-BPSA) for iris images are proposed in this paper. Different from SARA [39], M-BRA [5], and TV-SARA [4], reweighted analysis (RA) is not considered in this paper due to the long reconstruction time in the RA process and the main focus of this paper is to shorten the reconstruction time while keeping a good quality of the image. In addition, the presented research contributions are presented as follows:

- A novel compressed sampling for colored iris image is proposed by exploiting basis pursuit reconstruction method with average sparsity model.
- An analysis of sparsity basis in CS using sparsity averaging to enhance the performance of CS reconstruction and compared with the conventional CS basis, i.e., Haar, Daubechies 8 (Db8), and curvelet.
- An analysis of the proposed RGB-BPSA with the effect of resolutions and RGB layer.

- Performance analysis of RGB-BPSA in colored medical images with CS metrics.

The organization of this paper is listed as follows. The concept of compressed medical imaging is presented in Section II. A detailed explanation of CMI-SS-BPSA is presented in Section III. The results of the proposed CMI-SS-BPSA are shown in Section IV. Last, this paper is concluded in Section V.

II. COMPRESSED SAMPLING IN MEDICAL IMAGE

In compressed sampling [8], with an assumption of a signal to be sparse in some basis then the signal contains only k-number of non-zero value. In this paper, a medical image compression framework based on compressed sampling (CS) is studied, referred to as compressed medical imaging (CMI). In CMI, acquisition and reconstruction are performed. Acquisition is a process to measure the medical image where the measured signal samples are below the Nyquist-Shannon sampling theorem. Moreover, reconstruction is a process to recover an image from the measured signal.

A. CMI ACQUISITION

In CMI, an image as two-dimensional data is reshaped to a signal $\boldsymbol{s} \in \mathbb{R}^{n\times 1}$. Next, a signals are sparse and represented by some basis, i.e., a sparse signal $\boldsymbol{x}$ is the sparse representation of $\boldsymbol{s}$ with sparsity basis Ψ. A sparse domain is defined as $\boldsymbol{x} = \boldsymbol{\Psi s}$, where $\boldsymbol{\Psi} \in \mathbb{C}^{n\times n}$ and $\boldsymbol{s} \in \mathbb{C}^{n\times 1}$. The acquisition process in CMI is a process to measure a less m-number of sample from signal $\boldsymbol{x} \in \mathbb{C}^{n\times 1}$ using a sensing/measurement matrix $\boldsymbol{\Phi} \in \mathbb{C}^{m\times n}$. The result of this acquisition is a measured signal $\boldsymbol{y} \in \mathbb{C}^{m\times 1}$ and defined as

$$\boldsymbol{y} = \boldsymbol{\Phi x}. \tag{1}$$

The CMI acquisition becomes $\boldsymbol{y} = \boldsymbol{\Phi\Psi s}$, where $\boldsymbol{\Psi}$ and $\boldsymbol{\Phi}$ denote the sparsity basis and the acquisition matrix, respectively.

B. CMI RECONSTRUCTION

Reconstruction process is a process to recover $\boldsymbol{x}$ from $\boldsymbol{y}$ and $\boldsymbol{\Phi}$ as shown in Eq. (1). A signal $\boldsymbol{x}$ can be compressed following CS rule if the signal is sparse with k-sparse non-zero value. However, the reconstruction process is a convex problem as

$$\min_{\hat{\boldsymbol{x}}} \left\|\hat{\boldsymbol{x}}\right\|_1 \text{ s. t. } \|\boldsymbol{y} - \boldsymbol{\Phi}\bar{\boldsymbol{x}}\|_2 \leq \varepsilon, \tag{2}$$

where $\bar{\boldsymbol{x}}$ denotes the reconstructed sparse signal, $\|\cdot\|_2$ denotes ℓ_2 norm, ε denotes ℓ_2 norm upper bound, and $\|\cdot\|_1$ denotes ℓ_1 norm. From Eq. (1), given $\boldsymbol{\Phi}$, $\boldsymbol{\Psi}$, and $\boldsymbol{y}$, the optimization problem becomes

$$\hat{\boldsymbol{s}} = \min_{\boldsymbol{s}} \|\boldsymbol{s}\|_1 \text{ s. t. } \|\boldsymbol{y} - \boldsymbol{\Phi\Psi}\bar{\boldsymbol{s}}\|_2 \leq \varepsilon. \tag{3}$$

C. CMI METRICS

This section presents CMI metrics, i.e., compression ratio (CR), signal to noise ratio (SNR), and the structural similarity (SSIM) index. CR is calculated as

$$\text{CR} = \frac{n}{m}, \tag{4}$$

where n and m are the size of sparse signal $\boldsymbol{x}$ and measured signal $\boldsymbol{y}$, respectively. SNR is calculated as

$$\text{SNR} = \frac{1}{3}\sum_{i=1}^{3} 20\log_{10}\left(\frac{\|\boldsymbol{x}_i\|_2}{\left\|\boldsymbol{x}_i - \hat{\boldsymbol{x}}_i\right\|_2}\right), \tag{5}$$

where i denotes RGB color layers, $\boldsymbol{x}_i$ denotes the i-th original signal, and $\hat{\boldsymbol{x}}_i$ denotes the i-th reconstruction signal. SSIM is calculated as

$$\text{SSIM}(\boldsymbol{x}, \hat{\boldsymbol{x}}) = [\text{lum}(\boldsymbol{x}, \hat{\boldsymbol{x}})]^{\alpha} \cdot [\text{con}(\boldsymbol{x}, \hat{\boldsymbol{x}})]^{\beta} \cdot [\text{struc}(\boldsymbol{x}, \hat{\boldsymbol{x}})]^{\gamma}, \tag{6}$$

where lum, con, and struc denote the luminance, the contrast, and the structural of the image, respectively. The luminance, contrast, and structural are defined as

$$\begin{aligned} \text{lum}(\boldsymbol{x}, \hat{\boldsymbol{x}}) &= \frac{2\mu_{\boldsymbol{x}}\mu_{\hat{\boldsymbol{x}}} + \text{C}_1}{\mu_{\boldsymbol{x}}^2 + \mu_{\hat{\boldsymbol{x}}}^2 + \text{C}_1}, \\ \text{con}(\boldsymbol{x}, \hat{\boldsymbol{x}}) &= \frac{2\sigma_{\boldsymbol{x}}\sigma_{\hat{\boldsymbol{x}}} + \text{C}_2}{\sigma_{\boldsymbol{x}}^2 + \sigma_{\hat{\boldsymbol{x}}}^2 + \text{C}_2}, \\ \text{struc}(\boldsymbol{x}, \hat{\boldsymbol{x}}) &= \frac{\sigma_{\boldsymbol{x}\hat{\boldsymbol{x}}} + \text{C}_3}{\sigma_{\boldsymbol{x}}\sigma_{\hat{\boldsymbol{x}}} + \text{C}_3}, \end{aligned} \tag{7}$$

where $\mu_{\boldsymbol{x}}$ denotes the mean of pixels in original image, $\mu_{\hat{\boldsymbol{x}}}$ denotes the mean of the pixels in reconstruction image, $\sigma_{\boldsymbol{x}}$ denotes the standard deviations of pixels in original image, $\sigma_{\hat{\boldsymbol{x}}}$ denotes the standard deviations of pixels in reconstruction image, $\sigma_{\boldsymbol{x}\hat{\boldsymbol{x}}}$ denotes cross-covariance between $\boldsymbol{x}$ and $\hat{\boldsymbol{x}}$, C_3 is a default coefficient where $\text{C}_3 = \frac{\text{C}_2}{2}$, and $\alpha = \beta = \gamma = 1$ are exponent coefficients. SSIM becomes

$$\text{SSIM}(\boldsymbol{x}, \hat{\boldsymbol{x}}) = \frac{(2\mu_{\boldsymbol{x}}\mu_{\hat{\boldsymbol{x}}} + \text{C}_1)(2\sigma_{\boldsymbol{x}\hat{\boldsymbol{x}}} + \text{C}_2)}{\left(\mu_{\boldsymbol{x}}^2 + \mu_{\hat{\boldsymbol{x}}}^2 + \text{C}_1\right)\left(\sigma_{\boldsymbol{x}}^2 + \sigma_{\hat{\boldsymbol{x}}}^2 + \text{C}_2\right)}. \tag{8}$$

III. PROPOSED RGB-BPSA

In this paper, novel CMI for colored iris image is proposed which exploits basis pursuit with sparsity averaging (RGB-BPSA) as depicted in Fig. 1. First, a colored iris image $\boldsymbol{I} \in \mathbb{Z}^{N\times N\times 3}$ (denoted as colored original) is considered as input of the proposed method, where $N \times N$ denotes the resolution in pixels and the last dimension of the matrix denotes the RGB layers. Second, Red, Green, and Blue layers are obtained from original image. Third, preparation is performed to process Red, Green, and Blue layers. Fourth, spread spectrum (SS) sampling is performed using SS masking image to sample the prepared image and vector $\boldsymbol{y}$ is obtained. Fifth, sampled image is obtained from vector $\boldsymbol{y}$. Sixth, sparse basis (Ψ) is generated by sparsity averaging. Seventh, the CS reconstruction using BPSA is performed to recover $\boldsymbol{x}$ from the known $\boldsymbol{y}$, $\boldsymbol{\Psi}$, and $\boldsymbol{\Phi}$. Seventh, end of loop condition is checked, if the loop is not last layer (Blue layer), then continue to next loop. Last, if the loop is Blue layer loop, the process is finished with the result image.

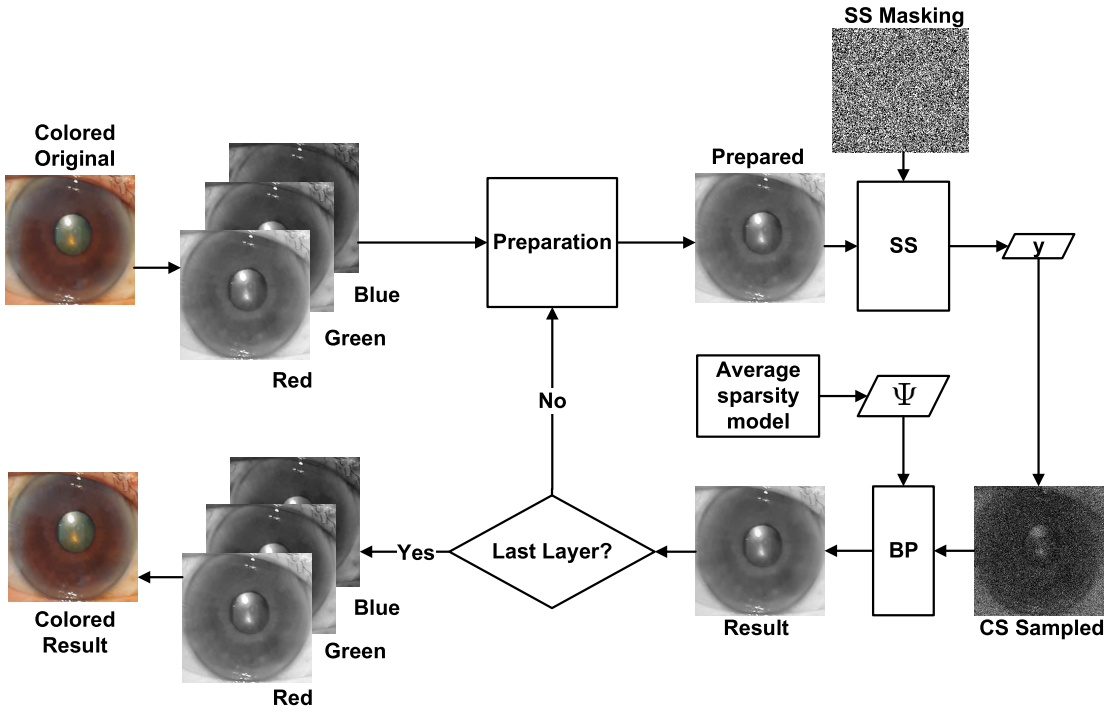

FIGURE 1. The graphical flow of the proposed RGB-BPSA.

Algorithm 1 RGB-BPSA

Input: Measured vector $\boldsymbol{y}$, SS mask $\boldsymbol{\Phi}$, and ε
Output: Reconstructed Iris Image $\hat{\boldsymbol{I}}$
Sparsity averaging basis Ψ
for $i \leftarrow 1$ **to** 3 **do**
  Initialization $j = 1$;
  while $j < j_{max}$ *and* $\alpha > \varepsilon$ **do**
    $\hat{\boldsymbol{x}}_i^{(j-1)} = \boldsymbol{\Psi}^{\dagger}\hat{\boldsymbol{x}}_i^{(j-1)}$;
    Compute BP solution $\Delta(\boldsymbol{y}, \boldsymbol{\Phi}, \varepsilon)$;
    $\hat{\boldsymbol{x}}_i^{(j)} = \Delta(\boldsymbol{y}, \boldsymbol{\Phi}, \varepsilon)$;
    Update $\alpha = \frac{\left\|\hat{\boldsymbol{x}}_i^{(j)} - \hat{\boldsymbol{x}}_i^{(j-1)}\right\|_1}{\left\|\hat{\boldsymbol{x}}_i^{(j-1)}\right\|_1}$;
    $j \leftarrow j + 1$;
  end
end
$\hat{\boldsymbol{I}} = \hat{\boldsymbol{x}}$;

Algorithm 1 presents RGB-BPSA. First, sparsity averaging generate basis Ψ. Second, 3 iterations are performed to reconstruct each layer of $\hat{\boldsymbol{x}}_i$ from sampled signal $\boldsymbol{y}$. Third, each i-iteration, BP solution (denoted as $\Delta(\boldsymbol{y}, \boldsymbol{\Phi}, \varepsilon)$ with $\boldsymbol{\Psi}$) is obtained. The iteration of BPSA is stop according to α less than $\varepsilon \in (0, 1)$, or $j = j_{max}$ is obtained.

A. PREPARATION

Each process of RGB loops is start with preparation process where the input is 1 layer image and the output is the prepared images. The preparation process consist of two process, i.e., pixel normalise and enforce positivity. The pixel normalise is a process to normalise the range oh pixel intensities to the normalized range as 0 and 1. While the enforce positivity is a process to remove the negative value after pixel normalise process. An visual example of preparation process is shown in Fig. 2(a).

B. SPREAD SPECTRUM SAMPLING

A CS approach using spread spectrum (SS) sampling is defined as

$$\boldsymbol{y} = \boldsymbol{\Phi}\boldsymbol{x} + \boldsymbol{w}, \tag{9}$$

where $\boldsymbol{\Phi} = \mathbf{MFA} \in \mathbb{C}^{m\times n}$ is the measurement matrix and $\boldsymbol{w}$ is input signal-to-noise ratio (ISNR). $\mathbf{M}$ is the mask image and modeled by a rectangular binary matrix $\mathbb{R}^{m\times n}$. $\mathbf{F}$ is the discrete Fourier transform coefficients and modeled by complex matrix $\mathbb{C}^{n\times n}$. $\mathbf{A}$ is spread spectrum matrix and modeled by a diagonal matrix $\mathbb{R}^{n\times n}$. $\mathbf{F}^{\mathrm{T}}\mathbf{M}^{\mathrm{T}}\mathbf{1}_M$ is the inverse transform of binary mask with matrix of ones $\mathbf{1}_M \in \mathbb{R}^M$. Fig. 2(b) show an visual example of SS process in terms of mask images and measured images after downsample process. The measurement is corrupted by complex Gaussian noise w and the associated ISNR is defined as

$$\mathrm{ISNR} = 20\log_{10}\left(\frac{\|\boldsymbol{y}_0\|_2}{\|\boldsymbol{w}\|_2}\right), \tag{10}$$

where y_0 denotes the clean measurement vector. This ISNR can be considered as noise in wireless networks transmission.

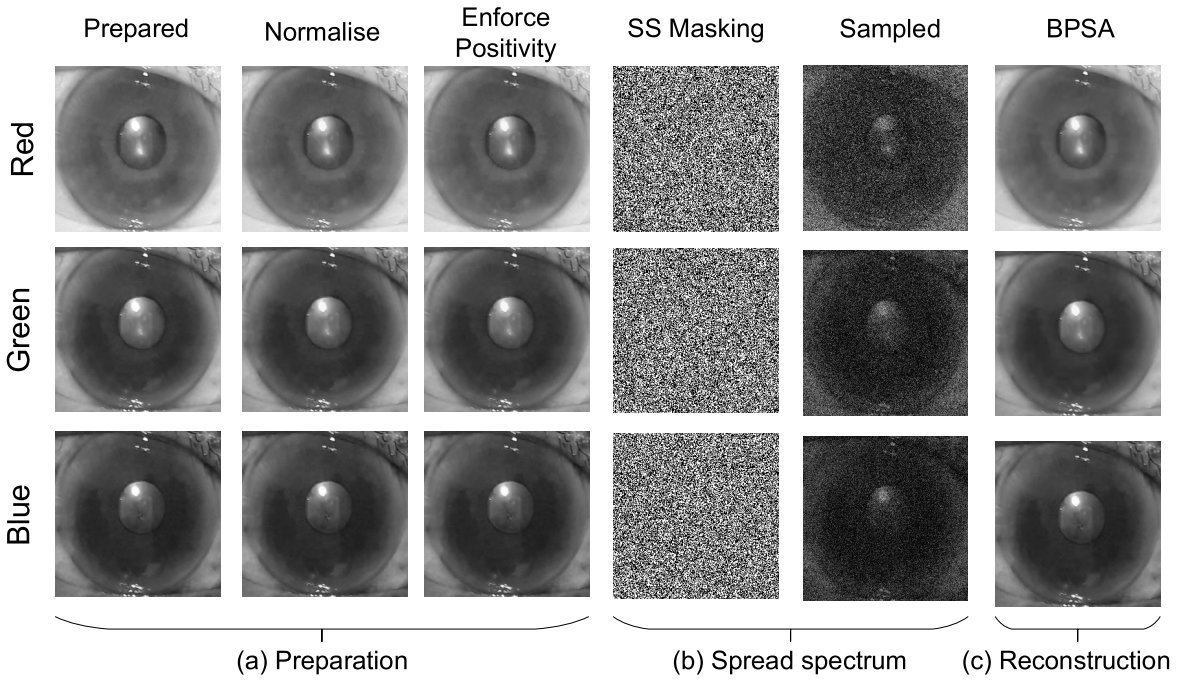

FIGURE 2. An visual of step in RGB-BPSA.

Moreover, an visual example of SS sampling is shown in Fig. 2(b).

C. SPARSITY AVERAGING (SA)

In sparsity averaging [38], $\boldsymbol{\Psi}$ denotes the sparse basis which is generated by averaging eight multiple wavelet bases with Daubechies (Db) mother wavelet filter and L-number of wavelet level decomposition. Furthermore, $\boldsymbol{\Psi}$ is defined as

$$\boldsymbol{\Psi} = \frac{1}{\sqrt{8}} \left[\boldsymbol{\Psi}_1, \boldsymbol{\Psi}_2, \ldots, \boldsymbol{\Psi}_8\right], \tag{11}$$

where $\boldsymbol{\Psi}_1$ is wavelet basis with Db1 mother wavelet and so on $\$\boldsymbol{\Psi}_8$ is wavelet basis with Db8 mother wavelet.

D. BASIS PURSUIT RECONSTRUCTION

In CS, the relation between sparsity basis $\boldsymbol{\Psi}$ and measurement matrix $\boldsymbol{\Phi}$ need to follow a restricted isometry property (RIP) [7]. CS problem is defined as

$$\min_{\bar{s}\in\mathbb{C}^m} \left\| \boldsymbol{\Psi}^{\dagger}\bar{s} \right\|_1 \quad \text{s.t.} \|\boldsymbol{y} - \boldsymbol{\Phi}\boldsymbol{\Psi}\bar{s}\|_2 \leq \varepsilon, \tag{12}$$

where $\boldsymbol{\Psi}^{\dagger}$ denotes an ad-joint operator of $\boldsymbol{\Psi}$. In this paper, 3 iterations of RGB image are performed and the example results of this process are shown in Fig. 2(c).

IV. EXPERIMENT

A. IRIS IMAGES

The iris images in this paper are obtained from the patients who had high cholesterol and acquired by one expert operator at the TelkomMedika hospital, Bandung, Indonesia [41], [42]. The test image is 90 colored iris images (RGB channel) with resolution 660 × 603 pixels in 8 bits *.BMP file format.

B. EXPERIMENT SCENARIO

Experiment scenario is presented to investigate RGB-BPSA using performance metrics in Section II-C. Firstly, colored iris image as original images is resized to $N \times N$ pixels. Then, mask image is generated according to CR to compress the original image using SS acquisition. Next, BPSA is performed to recover the compressed image and reconstructed image is obtained. Last, the performance metrics are obtained between the colored original and colored result image. The experiment scenarios are presented as follows

- The effect of decomposition level in wavelet; In this scenario, the resolutions is fixed using 64 × 64 pixels. This scenario investigates the effect of decomposition level in wavelet (l) for sparsity averaging.
- The effect of CR; In this scenario, the resolutions is fixed using 128 × 128 pixels. This scenario investigates the effect of CR in RGB-BPSA and RGB-BP with existing basis (i.e., haar, Db8, and curvelet).
- The effect of ISNR; In this scenario, CR is fixed using 0.5 and ISNR is investigated.
- The effect of resolutions; Different resolutions $N \times N$ of iris images are investigated, i.e., 64 × 64, 256 × 256, and 512 × 512 pixels.

C. HARDWARE AND SOFTWARE SPECIFICATIONS

In this paper, to implement the RGB-BPSA method in colored iris images, MATLAB R2020b is used for simulation and the hardware specifications are as follows: processor Intel(R) Core(TM) i&-8700 CPU @ 3.20GHz and installed RAM 16GB.

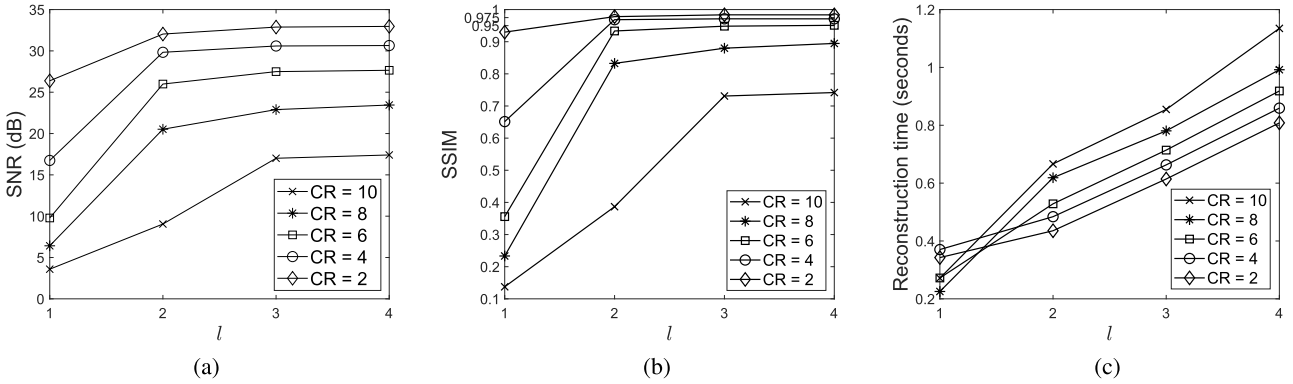

FIGURE 3. Performance metric results of RGB-BPSA with respects to *l*.

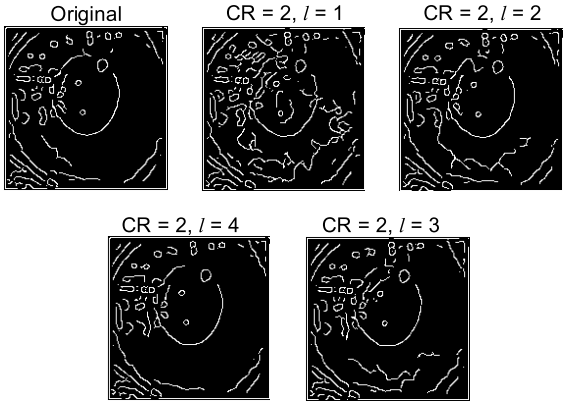

FIGURE 4. Figure of merit for an example of iris image with regard to *l*.

V. RESULTS

A. LEVEL OF WAVELET DECOMPOSITION

This Section presents the results of experiment scenario from Section IV-B to show the performance of RGB-BPSA. The performance comparison between the proposed RGB-BPSA, CS using BP with curvelet basis, Haar basis, and Daubechies 8 (Db8) basis are investigated using SNR and SSIM to show the visual quality, and also reconstruction time results.

The effect of decomposition level in wavelet is presented in Figs. 3(a), (b), and (c) for SNR, SSIM, and reconstruction time, respectively. Fig. 3(a) show the SNR results with the effect of $l = 1, 2, 3, 4$. SNR is calculated using (5) at CR $=$ 2, 4, 6, 8, 10. The results show that when l increases, SNR also increases. Targeting SNR $>$ 30 dB, is only achieved by $l > 1$ at CR $= 2$ and it is shown that iris image with resolution 64×64 pixels can compressed with good SNR using $l = 4$ at CR $= 2$. Furthermore, Table 1 presents SNR results in the form of mean with standard deviation.

Fig. 3(b) show the SSIM results with the effect of $l = 1, 2, 3, 4$. SSIM is calculated using (8) at CR $= 2, 4, 6, 8, 10$. The results show that when l increases, SSIM also increases. Targeting SSIM $>$ 0.95 dB, is only achieved by $l > 1$ at CR $= 2$ and it is shown that iris image with resolution 64×64 pixels can compressed with good SSIM using $l = 4$ at CR $= 2$. Furthermore, Table 3 presents SSIM results in the form of mean with standard deviation.

TABLE 1. SNR result w.r.t level in wavelet.

CR	Level			
	1	2	3	4
2	26.38 ± 0.33	32.03 ± 0.09	32.88 ± 0.13	32.96 ± 0.31
4	16.74 ± 0.27	29.83 ± 0.27	30.59 ± 0.14	30.64 ± 0.45
6	9.78 ± 0.04	25.98 ± 0.09	27.49 ± 0.16	27.65 ± 0.13
8	6.41 ± 0.08	20.52 ± 0.06	22.89 ± 0.59	23.45 ± 0.17
10	3.58 ± 0.06	9.05 ± 0.17	17.00 ± 0.02	17.40 ± 0.01

TABLE 2. Reconstruction time result w.r.t level in wavelet.

CR	Level			
	1	2	3	4
10	0.27 ± 0.01	0.66 ± 0.01	0.85 ± 0.01	1.13 ± 0.03
8	0.22 ± 0.00	0.61 ± 0.00	0.78 ± 0.02	0.99 ± 0.00
6	0.27 ± 0.00	0.52 ± 0.00	0.71 ± 0.01	0.91 ± 0.03
4	0.37 ± 0.00	0.48 ± 0.01	0.66 ± 0.01	0.85 ± 0.02
2	0.34 ± 0.01	0.43 ± 0.00	0.61 ± 0.00	0.80 ± 0.01

TABLE 3. SSIM result w.r.t level in wavelet.

CR	Level			
	1	2	3	4
2	0.92 ± 0.031	0.97 ± 0.001	0.98 ± 3.901	0.98 ± 0.001
4	0.65 ± 0.001	0.96 ± 0.001	0.97 ± 0.001	0.97 ± 0.011
6	0.35 ± 0.001	0.93 ± 0.001	0.94 ± 0.001	0.95 ± 0.001
8	0.23 ± 0.001	0.83 ± 0.001	0.87 ± 0.03	0.89 ± 0.01
10	0.13 ± 0.001	0.38 ± 0.001	0.73 ± 0.001	0.74 ± 0.001

Fig. 3(c) show the reconstruction time results with the effect of $l = 1, 2, 3, 4$. The results show that when l increases, SSIM also increases. Furthermore, Table 2 presents SSIM results in the form of mean with standard deviation.

Furthermore, figure of merit (FOM) is used to show the visual comparison between different results as shown in Fig. 4. The FOM shown that higher level and lower CR results gradually approach the original image.

B. COMPRESSION RATIO (CR)

In this subsection, the effect of CR is investigated and presented in Figs. 5(a), (b), and (c), for SNR, SSIM, and reconstruction time, respectively.

Fig. 5(a) show SNR results with regards to CR. Targeting SNR $>$ 20 dB, the proposed method achieves at all CR conditions and outperforms Curvelet, Haar, and Db8.

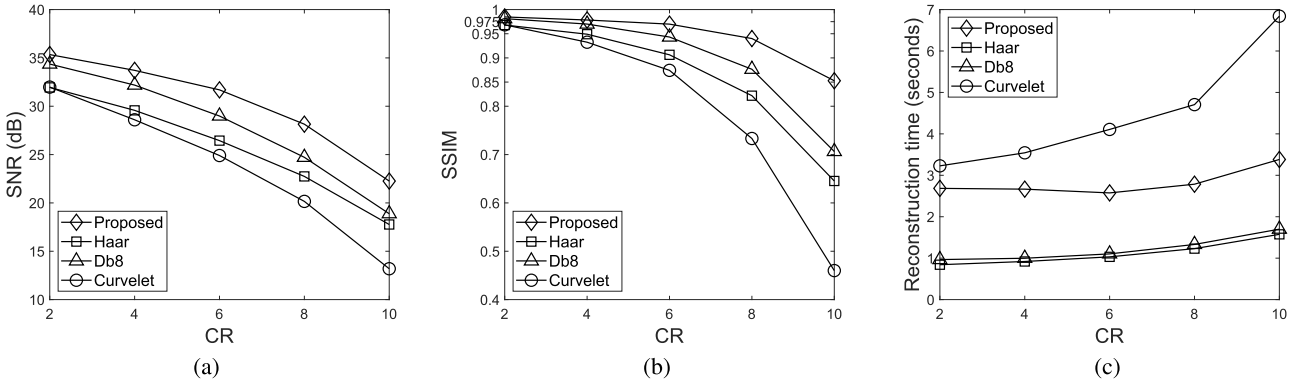

FIGURE 5. Performance metric results of RGB-BPSA with respects to CR.

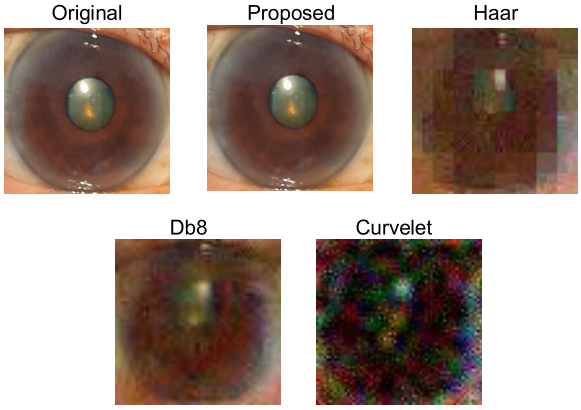

FIGURE 6. An example of iris image with different CS methods.

Next, Fig. 5(c) show SSIM with regards to CR, where the SSIM is calculated using (8). Targeting SSIM $>$ 0.95, the proposed method achieves at CR $\leq$ 6. The proposed method outperform all methods and it is shown that the highest CR $=$ 10 of the proposed method obtain SSIM $=$ 0.83.

Fig. 5(c) show reconstruction time with regards to CR $=$ 10, 8, 6, 4, 2 to investigate RGB-BPSA, BP with Haar basis, Db8 basis, and Curvelet basis. The reconstruction time results show that RGB-BPSA outperforms Curvelet CS methods with less reconstruction time at all CR conditions. The fastest and longest reconstruction time results are Haar and Curvelet, respectively. Even though Haar obtains the fastest reconstruction time, the SNR and SSIM of Haar basis is the second worst. With this condition, it is validated that RGB-BPSA with resolution 128 $\times$ 128 outperforms all existing CS methods in the view of SNR and SSIM, although the reconstruction time is two times longer from Haar and Db8.

Furthermore, an example of visual comparison between different results as shown in Fig. 6 with $N = 128$ at CR $= 10$. The proposed RGB-BPSA shows better visual and gradually approach the original image.

C. EFFECT OF ISNR

From Eq. (9), w denotes the complex Gaussian noise and related to ISNR. The proposed RGB-BPSA can solve two main problems of massive data generation, i.e., storage and transmission in wireless networks. To investigate the performance of RGB-BPSA, the effect of ISNR is presented with resolution 64 $\times$ 64 and CR $=$ 4. Figs. 7(a), (b) and (c) show the results of ASNR, SSIM, and reconstruction time, respectively.

Fig. 7(a) presents SNR results with the effect of ISNR. Targeting SNR $\geq$ 20 dB, CR $\leq$ 8 is recommended at all ISNR. The ASNR of CR $=$ 10 is saturated around 17 dB at all ISNR, the ASNR of CR $=$ 8 is saturated around 23 dB at ISNR $\geq$ 20 dB, the ASNR of CR $=$ 6 is saturated around 28 dB at ISNR $\geq$ 30 dB, the ASNR of CR $=$ 4 is saturated around 31 dB at ISNR $\geq$ 40 dB, and the ASNR of CR $=$ 2 is saturated around 34 dB at ISNR $\geq$ 50 dB. It is show that lower CR is required for lower ISNR.

Fig. 7(b) presents SSIM results with the effect of ISNR. Targeting SSIM $\geq$ 0.9, CR $\leq$ 6 is recommended at ISNR $>$ 10 dB. The SSIM of CR $=$ 10 is saturated around 0.74 at all ISNR, the ASNR of CR $=$ 8 is saturated around 0.88 at ISNR $\geq$ 20 dB, the ASNR of CR $=$ 6 is saturated around 0.95 at ISNR $\geq$ 30 dB, the ASNR of CR $=$ 4 is saturated around 0.97 at ISNR $\geq$ 30 dB, and the ASNR of CR $=$ 2 is saturated around 0.98 at ISNR $\geq$ 30 dB. It is show that lower CR is required for lower ISNR.

Furthermore, Fig. 7(c) presents reconstruction time results with regards to ISNR. The proposed method outperforms BPSA with faster reconstruction time at all ISNR conditions.

D. RESOLUTIONS

The effect of resolutions to SNR, SSIM, and reconstruction time are presented in Fig. 8(a), (b), (c), respectively. The solid lines denote 64 $\times$ 64 pixels, dash lines denote 256 $\times$ 256 pixels, and dash-dot lines denote 256 $\times$ 256 pixels. The comparison between RGB-BPSA (Proposed) and RGB-BP with Db8 basis is shown to show the SNR, SSIM, and reconstruction time. The results of the proposed method with $N = 256, 512$ achieve SNR $>$ 30 dB and SSIM $>$ 0.93 at CR $\leq$ 8. From the SNR and SSIM, RGB-BPSA outperforms RGB-BP with Db8 basis while the reconstruction time increases 2$\times$ than RGB-BP with Db8. The results of

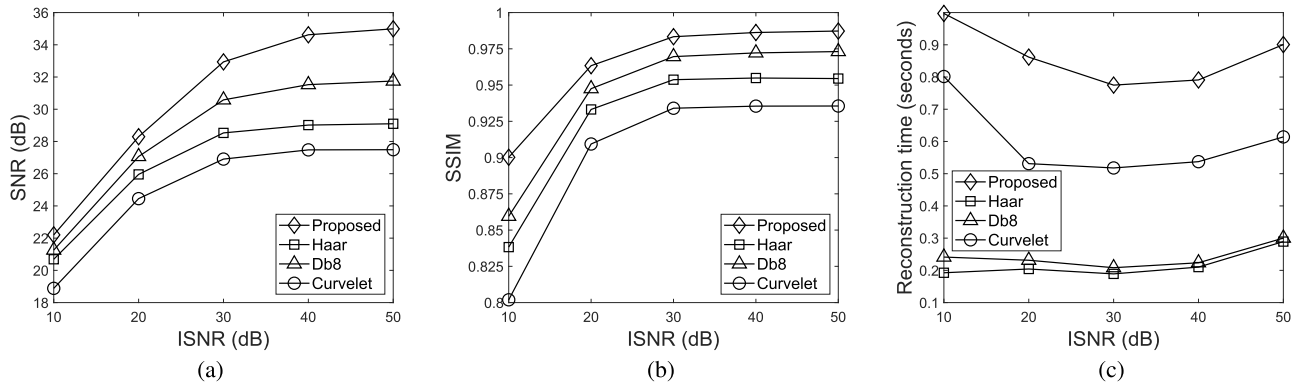

FIGURE 7. Performance metric results of RGB-BPSA with respects to ISNR.

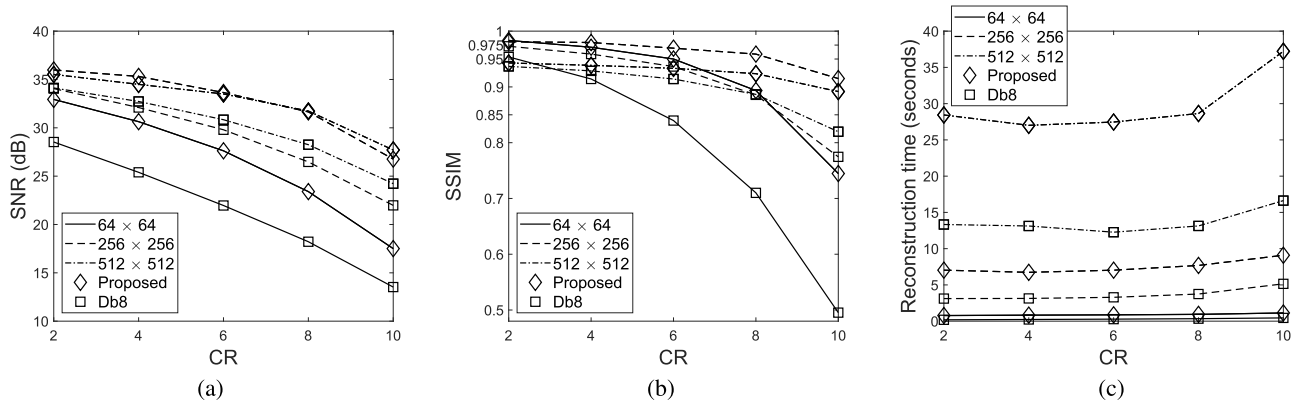

FIGURE 8. Performance metric results of RGB-BPSA with respects to resolutions.

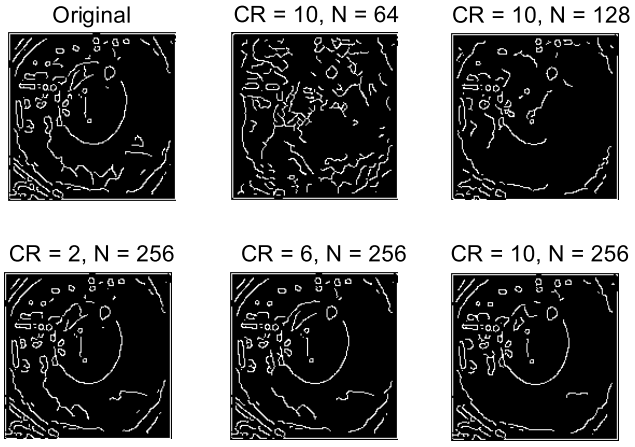

FIGURE 9. Figure of merit for an example of iris image with regard to *N*.

resolutions $N = 64$ shows that the proposed RGB-BPSA achieve $SNR > 30$ dB and SSIM > 0.95 at CR ≤ 4. The reconstruction time of $N = 64$ shows the same trends, the RGB-BPSA achieves longer time with ratio $2\times$ than RGB-BP with Db8.

Furthermore, figure of merit (FOM) is used to show the visual comparison between different results as shown in Fig. 8. The FOM shown that higher resolution ($N = 256$) and lower CR results gradually approach the original image.

VI. CONCLUSION

This paper have proposed novel CS of colored iris image using spread spectrum sampling for acquisition and basis pursuit with sparsity averaging (BPSA) for reconstruction. The sparsity averaging basis improves the performance of CS reconstruction quantitatively which is measured by SNR and SSIM on colored iris images. The proposed RGB-BPSA outperforms CS using BP with curvelet, haar, and Db8 basis and can be compressed until CR ≤ 6 in SNR > 30 and SSIM > 0.95 using resolution more than 128×128 pixels. The cost of the proposed RGB-BPSA is reconstruction time, where it increases two times than haar and Db8, while the reconstruction time of RGB-BPSA outperforms curvelet basis.

For future work, one can explore but not be limited, the efficiency of the presented CS method considering higher image resolutions (i.e. 1024×1024 pixels). In addition, the performance of CS to the noise can extend to another type of noise and existing noise removal methods [43]–[45].

REFERENCES

[1] A. P. Dhawan, B. H. Huang, and D.-S. Kim, *Principles and Advanced Methods in Medical Imaging and Image Analysis*. Singapore: World Scientific, 2008.

[2] X. Zeng, S. Tong, Y. Lu, L. Xu, and Z. Huang, "Adaptive medical image deep color perception algorithm," *IEEE Access*, vol. 8, pp. 56559–56571, 2020.

[3] E. D. Angelini, O. Clatz, E. Mandonnet, E. Konukoglu, L. Capelle, and H. Duffau, "Glioma dynamics and computational models: A review of segmentation, registration, and in silico growth algorithms and their clinical applications," *Current Med. Imag. Rev.*, vol. 3, no. 4, pp. 262–276, 2007.
[4] T. Rahim, L. Novamizanti, I. N. A. Ramatryana, S. Y. Shin, and D. S. Kim, "Total variant based average sparsity model with reweighted analysis for compressive sensing of computed tomography," *IEEE Access*, vol. 9, pp. 119158–119170, 2021.
[5] T. Rahim, L. Novamizanti, I. N. Apraz Ramatryana, and S. Y. Shin, "Compressed medical imaging based on average sparsity model and reweighted analysis of multiple basis pursuit," *Computerized Med. Imag. Graph.*, vol. 90, Jun. 2021, Art. no. 101927.
[6] T. W. Cabral, M. Khosravy, F. M. Dias, H. L. M. Monteiro, M. A. A. Lima, L. R. M. Silva, R. Naji, and C. A. Duque, "Compressive sensing in medical signal processing and imaging systems," in *Sensors for Health Monitoring*. Amsterdam, The Netherlands: Elsevier, 2019, pp. 69–92.
[7] D. L. Donoho, "Compressed sensing," *IEEE Trans. Inf. Theory*, vol. 52, no. 4, pp. 1289–1306, Apr. 2006.
[8] E. J. Candès and M. B. Wakin, "An introduction to compressive sampling," *IEEE Signal Process. Mag.*, vol. 25, no. 2, pp. 21–30, Mar. 2008.
[9] L. Wang, L. Li, L. Jin, L. Jing, B. B. Gupta, and L. Xia, "Compressive sensing of medical images with confidentially homomorphic aggregations," *IEEE Internet Things J.*, vol. 6, no. 2, pp. 1402–1409, Apr. 2019.
[10] M. Jacob, J. C. Ye, L. Ying, and M. Doneva, "Computational MRI: Compressive sensing and beyond [from the guest editors]," *IEEE Signal Process. Mag.*, vol. 37, no. 1, pp. 21–23, Jan. 2020.
[11] L. Stankovic and M. Brajovic, "Analysis of the reconstruction of sparse signals in the DCT domain applied to audio signals," *IEEE/ACM Trans. Audio, Speech, Lang. Process.*, vol. 26, no. 7, pp. 1220–1235, Jul. 2018.
[12] L. Stanković, M. Brajović, I. Stanković, C. Ioana, and M. Daković, "Reconstruction error in nonuniformly sampled approximately sparse signals," *IEEE Geosci. Remote Sens. Lett.*, vol. 18, no. 1, pp. 28–32, Jan. 2021.
[13] L. Stankovic, I. Stankovic, and M. Dakovic, "Nonsparsity influence on the ISAR recovery from reduced data [correspondence]," *IEEE Trans. Aerosp. Electron. Syst.*, vol. 52, no. 6, pp. 3065–3070, Dec. 2016.
[14] Z. Wang, M. He, Z. Ye, K. Xu, Y. Nian, and B. Huang, "Reconstruction of hyperspectral images from spectral compressed sensing based on a multitype mixing model," *IEEE J. Sel. Topics Appl. Earth Observ. Remote Sens.*, vol. 13, pp. 2304–2320, 2020.
[15] Q. Sun, "Recovery of sparsest signals via ℓ_q-minimization," *Appl. Comput. Harmon. Anal.*, vol. 32, no. 3, pp. 329–341, 2012.
[16] L. Wang, Y. Feng, Y. Gao, Z. Wang, and M. He, "Compressed sensing reconstruction of hyperspectral images based on spectral unmixing," *IEEE J. Sel. Topics Appl. Earth Observ. Remote Sens.*, vol. 11, pp. 1266–1284, 2018.
[17] S. Yang, M. Wang, P. Li, L. Jin, B. Wu, and L. Jiao, "Compressive hyperspectral imaging via sparse tensor and nonlinear compressed sensing," *IEEE Trans. Geosci. Remote Sens.*, vol. 53, no. 11, pp. 5943–5957, Nov. 2015.
[18] R. van Sloun, A. Pandharipande, M. Mischi, and L. Demi, "Compressed sensing for ultrasound computed tomography," *IEEE Trans. Biomed. Eng.*, vol. 62, no. 6, pp. 1660–1664, Jun. 2015.
[19] S. Hashemi, S. Beheshti, P. R. Gill, N. S. Paul, and R. S. Cobbold, "Accelerated compressed sensing based ct image reconstruction," *Comput. Math. methods Med.*, vol. 2015, Jun. 2015, Art. no. 161797.
[20] Z. Zhu, K. Wahid, P. Babyn, D. Cooper, I. Pratt, and Y. Carter, "Improved compressed sensing-based algorithm for sparse-view CT image reconstruction," *Comput. Math. Methods Med.*, vol. 2013, pp. 1–15, May 2013.
[21] S. Hua, M. Ding, and M. Yuchi, "Sparse-view ultrasound diffraction tomography using compressed sensing with nonuniform FFT," *Comput. Math. Methods Med.*, vol. 2014, pp. 1–13, Jun. 2014.
[22] G.-H. Chen, J. Tang, and S. Leng, "Prior image constrained compressed sensing (PICCS): A method to accurately reconstruct dynamic CT images from highly undersampled projection data sets," *Med. Phys.*, vol. 35, no. 2, pp. 660–663, 2008.
[23] X. Li and S. Luo, "A compressed sensing-based iterative algorithm for CT reconstruction and its possible application to phase contrast imaging," *Biomed. Eng. OnLine*, vol. 10, no. 1, p. 73, 2011.
[24] J. Huang, S. Zhang, and D. Metaxas, "Efficient MR image reconstruction for compressed MR imaging," *Med. Image Anal.*, vol. 15, no. 5, pp. 670–679, Oct. 2011.
[25] Y. Liu, Z. Zhan, J.-F. Cai, D. Guo, Z. Chen, and X. Qu, "Projected iterative soft-thresholding algorithm for tight frames in compressed sensing magnetic resonance imaging," *IEEE Trans. Med. Imag.*, vol. 35, no. 9, pp. 2130–2140, Sep. 2016.
[26] B. Zhao, J. P. Haldar, A. G. Christodoulou, and Z.-P. Liang, "Image reconstruction from highly undersampled (k, t)-space data with joint partial separability and sparsity constraints," *IEEE Trans. Med. Imag.*, vol. 31, no. 9, pp. 1809–1820, Sep. 2012.
[27] Q. Liu, S. Wang, K. Yang, J. Luo, Y. Zhu, and D. Liang, "Highly undersampled magnetic resonance image reconstruction using two-level Bregman method with dictionary updating," *IEEE Trans. Med. Imag.*, vol. 32, no. 7, pp. 1290–1301, Jul. 2013.
[28] S. Wang, Z. Su, L. Ying, X. Peng, S. Zhu, F. Liang, D. Feng, and D. Liang, "Accelerating magnetic resonance imaging via deep learning," in *Proc. IEEE 13th Int. Symp. Biomed. Imag. (ISBI)*, Apr. 2016, pp. 514–517.
[29] J. Sun, H. Li, and Z. Xu, "Deep ADMM-Net for compressive sensing MRI," in *Proc. Adv. Neural Inf. Process. Syst.*, vol. 29, 2016.
[30] T. M. Quan, T. Nguyen-Duc, and W.-K. Jeong, "Compressed sensing MRI reconstruction using a generative adversarial network with a cyclic loss," *IEEE Trans. Med. Imag.*, vol. 37, no. 6, pp. 1488–1497, Jun. 2018.
[31] M. Mardani, E. Gong, and J. Cheng, "Deep generative adversarial neural Networks for compressive sensing MRI," *IEEE Trans. Med. Imag.*, vol. 38, no. 1, pp. 167–179, Jan. 2019.
[32] J. Xue, L. Yin, Z. Lan, M. Long, G. Li, Z. Wang, and X. Xie, "3D DCT based image compression method for the medical endoscopic application," *Sensors*, vol. 21, no. 5, p. 1817, Mar. 2021.
[33] P. Turcza and M. Duplaga, "Low-power image compression for wireless capsule endoscopy," in *Proc. IEEE Int. Workshop Imag. Syst. Techn.*, May 2007, pp. 1–4.
[34] L.-R. Dung, Y.-Y. Wu, H.-C. Lai, and P.-K. Weng, "A modified H.264 intra-frame video encoder for capsule endoscope," in *Proc. IEEE Biomed. Circuits Syst. Conf.*, Nov. 2008, pp. 61–64.
[35] T. H. Khan and K. A. Wahid, "Lossless and low-power image compressor for wireless capsule endoscopy," in *Proc. VLSI Design*, 2011, pp. 1–13.
[36] M.-C. Lin, L.-R. Dung, and P.-K. Weng, "An ultra-low-power image compressor for capsule endoscope," *Biomed. Eng.*, vol. 5, no. 1, pp. 1–8, Dec. 2006.
[37] T. N. Canh and B. Jeon, "Multi-scale deep compressive imaging," *IEEE Trans. Comput. Imag.*, vol. 7, pp. 86–97, 2020.
[38] R. E. Carrillo, J. D. McEwen, and Y. Wiaux, "Sparsity averaging reweighted analysis (SARA): A novel algorithm for radio-interferometric imaging," *Mon. Not. Roy. Astron. Soc.*, vol. 426, no. 2, pp. 1223–1234, 2012.
[39] R. E. Carrillo, J. D. McEwen, D. Van De Ville, J.-P. Thiran, and Y. Wiaux, "Sparsity averaging for compressive imaging," *IEEE Signal Process. Lett.*, vol. 20, no. 6, pp. 591–594, May 2013.
[40] I. N. A. Ramatryana, T. Rahim, and S. Y. Shin, "Compressed medical imaging using doubly parseval frame sparsity averaging," in *Proc. Korea Telecommun. Soc. Conf.*, 2020, pp. 206–207.
[41] S. N. Andana, L. Novamizanti, and I. N. A. Ramatryana, "Measurement of cholesterol conditions of eye image using fuzzy local binary pattern (FLBP) and linear regression," in *Proc. IEEE Int. Conf. Signals Syst. (ICSigSys)*, Jul. 2019, pp. 79–84.
[42] C. A. Nurbani, L. Novamizanti, I. N. Ramatryana, and N. P. D. Wardana, "Measurement of cholesterol levels through eye based on co-occurrence matrix on android," in *Proc. IEEE Asia Pacific Conf. Wireless Mobile (APWiMob)*, Nov. 2019, pp. 88–93.
[43] A. Khmag, A. R. Ramli, S. J. Hashim, and S. A. R. Al-Haddad, "Additive noise reduction in natural images using second-generation wavelet transform hidden Markov models," *IEEJ Trans. Electr. Electron. Eng.*, vol. 11, no. 3, pp. 339–347, May 2016.
[44] G. Chen, F. Zhu, and P. A. Heng, "An efficient statistical method for image noise level estimation," in *Proc. IEEE Int. Conf. Comput. Vis. (ICCV)*, Dec. 2015, pp. 477–485.
[45] A. Khmag, S. A. R. Al Haddad, R. A. Ramlee, N. Kamarudin, and F. L. Malallah, "Natural image noise removal using nonlocal means and hidden Markov models in transform domain," *Vis. Comput.*, vol. 34, no. 12, pp. 1661–1675, Dec. 2018.

TARIQ RAHIM (Member, IEEE) received the B.Sc. degree from the COMSAT Institute of Information and Technology, Pakistan, the M.S. degree from the Beijing Institute of Technology, China, and the Ph.D. degree in IT convergence engineering from the Wireless and Emerging Network System Laboratory (WENS Lab), Kumoh National Institute of Technology (KIT), South Korea. He is currently working as a Postdoctoral Fellow and a Researcher at ICT-CRC, KIT. His research interests mainly include signal processing, image processing, medical image analysis, deep learning, video processing, and quality of services of high frame rate videos.

RITA MAGDALENA received the Bachelor of Engineering degree in electrical engineering from North Sumatera University, Indonesia, in 1987, and the Master of Engineering degree in electrical engineering from the Bandung Institute of Technology, Indonesia, in 2001. She has been working as a Lecturer with Telkom University, since 1999. Her current research interests include signal processing and artificial intelligence.

I PUTU AGUS EKA PRATAMA received the bachelor's degree in informatics from the Institut Teknologi Telkom and the master's degree in informatics from the Institut Teknologi Bandung (ITB). He has been working as a Researcher and a Lecturer at the Information Network and System (INS) Research Laboratory, ITB. Since 2015, he has been a Lecturer at the Department of Information Technology, Faculty of Engineering, Udayana University. He has been an ICT Consultant and the author of 12 ICT books, since 2014. His research interests include smart city, big data, computer networks, computer security, linux, and intelligent transportation systems.

LEDYA NOVAMIZANTI (Graduate Student Member, IEEE) received the Bachelor of Science (S.Si.) degree in mathematics from Andalas University, Indonesia, in 2005, and the Master of Engineering (M.T.) degree in electrical engineering from Telkom University, Indonesia, in 2008. She has been working as a Lecturer at Telkom University, since 2010. Her current research interests include signal processing, computer vision, pattern recognition, and artificial intelligence.

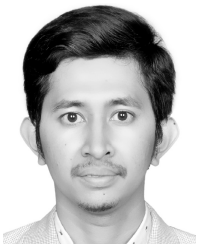

I NYOMAN APRAZ RAMATRYANA (Graduate Student Member, IEEE) received the bachelor's degree in telecommunication engineering and the master's degree in electrical and telecommunication engineering from the Telkom Institute of Technology (currently known as Telkom University), Indonesia, in 2010 and 2014, respectively. He is currently pursuing the Ph.D. degree in IT convergence engineering with the Kumoh National Institute of Technology, South Korea. His areas of expertise are signal processing, artificial intelligence (AI), wireless communications, and computer vision. His research interests include random access (RA), Raptor coding, non-orthogonal multiple access (NOMA), multiple-input multiple-output (MIMO) antenna, compressed imaging, medical imaging, and deep learning (DL).

SOO YOUNG SHIN (Senior Member, IEEE) received the B.S., M.S., and Ph.D. degrees in electrical engineering and computer science from Seoul National University, South Korea, in 1999, 2001, and 2006, respectively. He was a Visiting Scholar at the FUN Laboratory, University of Washington, USA, from July 2006 to June 2007. After three years working at the WiMAX Design Laboratory, Samsung Electronics, he has been an Associate Professor with the School of Electronics, Kumoh National Institute of Technology, since September 2010. His research interests include wireless LAN, WPAN, WBAN, wireless mesh networks, sensor networks, coexistence among wireless networks, industrial and military networks, cognitive radio networks, and next generation mobile wireless broadband networks.

DONG SEONG KIM (Senior Member, IEEE) received the Ph.D. degree in electrical and computer engineering from Seoul National University, Seoul, South Korea, in 2003. From 1994 to 2003, he worked as a full-time Researcher at ERC-ACI, Seoul National University. From March 2003 to February 2005, he worked as a Postdoctoral Researcher at the Wireless Network Laboratory, School of Electrical and Computer Engineering, Cornell University, NY, USA. From 2007 to 2009, he was a Visiting Professor with the Department of Computer Science, University of California, Davis, CA, USA. He is currently the Director of the KIT Convergence Research Institute and the ICT Convergence Research Center (ITRC and NRF Advanced Research Center Program) supported by Korean Government at the Kumoh National Institute of Technology. His current main research interests include real-time IoT and smart platform, industrial wireless control networks, networked embedded systems, and fieldbus. He is a Senior Member of ACM.